Integrated CO_2 capture and selective conversion to syngas using transition-metal-free Na/Al_2O_3 dual-function material

Sasayama, Tomone; Kosaka, Fumihiko; Liu, Yanyong; Yamaguchi, Toshiaki; Chen, Shih Yuan; Mochizuki, Takehisa; Urakawa, Atsushi; Kuramoto, Koji

DOI
10.1016/j.jcou.2022.102049

Publication date
2022

Document Version
Final published version

Published in
Journal of CO2 Utilization

Journal of CO2 Utilization 60 (2022) 102049

Contents lists available at ScienceDirect

Journal of CO2 Utilization

journal homepage: www.elsevier.com/locate/jcou

Integrated CO_2 capture and selective conversion to syngas using transition-metal-free Na/Al_2O_3 dual-function material

Tomone Sasayama [a], Fumihiko Kosaka [a,*], Yanyong Liu [a], Toshiaki Yamaguchi [a], Shih-Yuan Chen [a], Takehisa Mochizuki [a], Atsushi Urakawa [b], Koji Kuramoto [a]

[a] National Institute of Advanced Industrial Science and Technology (AIST), 16-1 Onogawa, Tsukuba, Ibaraki 305-8569, Japan
[b] Delft University of Technology, Van der Maasweg 9, 2629 Hz Delft, The Netherlands

ARTICLE INFO

Keywords:
CO_2 capture
CO_2 utilization
Dual-function material
Reverse water gas shift
Syngas

ABSTRACT

Integrated CO_2 capture and conversion (ICCC) using dual-function materials (DFMs) is one of the key technologies for addressing critical global environmental and energy issues. DFMs generally consist of alkali or alkaline earth metals for CO_2 capture and transition metal catalysts for CO_2 conversion. In this study, we studied the ICCC to CO using transition-metal-free DFMs to demonstrate their potential to directly produce syngas from atmospheric-level CO_2. Among the DFMs prepared herein, Na/Al_2O_3 exhibited excellent performance and achieved a CO_2 conversion exceeding 90% and CO selectivity exceeding 95% at a reaction temperature of 450–500 °C. Na/Al_2O_3 maintained its capture and conversion capacity throughout a 50-cycle stability test without significant deactivation. Furthermore, in the scale-up experiments using Na/Al_2O_3 DFM, a syngas-like mixture an H_2/CO molar ratio of 3.3 (48.1 vol% H_2 and 14.5 vol% CO) was directly obtained from 400 ppm CO_2. These results suggest that ICCC using the transition-metal-free Na/Al_2O_3 DFM may be practicable provided the CO_2 capture capacity of the DFM is further improved while maintaining the aforementioned advantages.

1. Introduction

The development of carbon dioxide capture, utilization and storage (CCUS) technologies is essential for addressing critical global environmental and energy issues. CCUS technologies capture CO_2 from industrial exhaust gases or the atmosphere and convert it into value-added products such as fuels and chemicals, or store it safely underground [1–6]. In general, CO_2 capture and utilization/storage are performed in physically separate processes. Therefore, energy- and cost-intensive operations such as CO_2 purification, compression, and transportation to a utilization/storage site are required following CO_2 capture [7,8].

Recently, integrated CO_2 capture and conversion (ICCC) processes using dual-function materials (DFMs) have emerged as advantageous alternatives for CCUS [9–12]. DFMs generally consist of alkali or alkaline earth metals for CO_2 capture and transition metal catalysts for CO_2 conversion. In the initial step of an ICCC process, a CO_2-containing gas is supplied to a reactor packed with the DFM, as illustrated in Fig. 1. CO_2 is selectively captured by the DFM, mainly via carbonation (Eq. 1), and the CO_2-free gas exits the reactor.

$$M_xO + CO_2 \rightleftharpoons M_xCO_3 \quad (1)$$

Subsequently, the gas stream is switched to renewable H_2. CO_2 is released by the reverse reaction of Eq. 1, namely decarbonation, and converted into fuels and chemicals through reaction with H_2. The transformation may take place directly through an active surface intermediate without releasing CO_2. The advantage of ICCC over conventional CCUS is that energy-and cost-intensive operations such as purification and transportation are obviated, and dilute CO_2 can be directly converted into target chemicals [10,12].

The majority of studies on ICCC using DFMs focus on the methanation of CO_2 by the Sabatier reaction (Eq. 2).

$$CO_2 + 4\,H_2 \rightleftharpoons CH_4 + 2\,H_2O \quad (2)$$

Farrauto's research group pioneered ICCC using Ru, $CaO/\gamma\text{-}Al_2O_3$ as a DFM [13]. Subsequently, new types of DFMs have been proposed, including those containing inexpensive Ni catalysts [14–16] and those in

Abbreviations: DFM, dual-function material; CCUS, carbon dioxide capture, utilization and storage; ICCC, integrated CO_2 capture and conversion; RWGS, reverse water gas shift.

* Corresponding author.
E-mail address: f.kosaka@aist.go.jp (F. Kosaka).

https://doi.org/10.1016/j.jcou.2022.102049
Received 25 February 2022; Received in revised form 21 April 2022; Accepted 29 April 2022
Available online 13 May 2022

which the sorbent (CO_2) and the transition metal catalyst are directly combined by the sol-gel method in the absence of a support [17,18]. In addition to fundamental and mechanistic in situ and operando studies [19–21], industrially important kinetic analyses [22,23] are ongoing. However, due to the chemical stability of CH_4, CO_2-derived CH_4 might be utilized mainly as a fuel gas without further conversion.

In contrast, several studies have attempted to convert CO_2 into CO by the reverse water gas shift (RWGS, Eq. 3) reaction [24–30].

$$CO_2 + H_2 \rightleftharpoons CO + H_2O \quad (3)$$

Via the RWGS reaction, a mixture of CO and H_2, named syngas, can theoretically be obtained by completely converting CO_2 with a stoichiometric excess of H_2 and removing the moisture by condensation. In particular, syngas having an H_2/CO ratio of 2–3 is a feedstock for the well-developed methanol synthesis (Eq. 4) and Fischer-Tropsch synthesis (Eq. 5) for the production of liquid fuels or chemicals.

$$CO + 2\,H_2 \rightarrow CH_3OH \quad (4)$$

$$n\mathrm{CO} + (2n{+}1)\mathrm{H_2} \rightarrow \mathrm{C}_n\mathrm{H}_{2n+2} + n\mathrm{H_2O} \quad (5)$$

Therefore, the conversion of captured CO_2 into syngas could be a more attractive and versatile option than converting it into CH_4.

In ICCC processes focusing on the RWGS, DFMs with and without supports can both be utilized. Examples of the former include FeCrCu/K/MgO-Al_2O_3 [24] and K/Ba-promoted Cu/Al_2O_3 [25], while examples of the latter include $Fe_5Co_5Mg_{10}CaO$ [28] and Ni/CaO [27,30]. In some studies, ICCC has been performed in the absence of transition metals using unsupported CaO [18,29]. Although conducting ICCC using solely CaO reduces the cost of the DFM, the formation of CO is slow, and the CO_2 capture and release temperatures are 600–700 °C. The cycle stability at such elevated temperatures is low. Although a transition-metal-free DFM in which only alkali or alkaline earth metals are carried on the support would have a smaller CO_2 capture capacity, it would overcome the aforementioned shortcomings. Such materials have been studied only as CO_2 sorbents [31–33] and not as DFMs.

In addition, the low concentration of the CO generated is a common shortcoming of ICCC processes based on the RWGS reaction. Compared to the conventional process which employs a simultaneous supply of CO_2 and H_2, ICCC processes using DFMs exhibit higher CO_2 conversion because of the kinetically driven process [12]. However, the molar ratio of unreacted H_2 to the produced CO is excessive for syngas. The ability of ICCC processes using DFMs to achieve a practical H_2/CO ratio for syngas remains unproven.

In this study, transition-metal-free DFMs, in which only CO_2 sorbents such as Na, K, or Ca was dispersed over an alumina support, were prepared, and evaluated for ICCC to CO. Initially, the amount of CO_2 captured, the conversion of captured CO_2, and selectivity for CO were compared for screening of DFM performance. Thereafter, the effects of the reaction temperature throughout the ICCC experiments and the H_2 flow rate in the conversion step were discussed, and the stability of the DFM was investigated. Finally, the practical value of the process was evaluated by operating the process on a 60 times larger scale using the best performing DFM with 5 vol% and 400 ppm CO_2 to verify a production of syngas with a practical H_2/CO ratio under model flue-gas or direct air capture modes of operation.

2. Materials and methods

2.1. Preparation of DFM

γ-Al_2O_3 (Neobead MSC#300, Mizusawa Industrial Chemicals, Ltd.) was used as a support for the DFM. Na_2CO_3, K_2CO_3, and $Ca(NO_3)_2 \cdot 4\,H_2O$ (guaranteed reagent, Fujifilm Wako Pure Chemical Corp.) were used as precursors. Table 1 lists the DFMs prepared. All the DFMs were prepared by the impregnation method as follows: Initially, γ-Al_2O_3 was impregnated with an aqueous solution containing a predetermined amount of one of the precursors, and subsequently dried at 110 °C for 12 h. The dried samples were calcined in air at 550 °C for 4 h to obtain Na/Al_2O_3, K/Al_2O_3, and Ca/Al_2O_3, according to the selection of precursor. The alkali and alkaline earth metal loading was set at 1.5 mmol per 1 g of DFM in carbonate form.

Table 1
Compositions of the as-prepared DFMs.

DFM	support	precursor	loading[a]	
			[wt%]	[mmol/g-DFM]
Na/Al_2O_3	γ-Al_2O_3	Na_2CO_3	16	1.5
K/Al_2O_3	ditto	K_2CO_3	21	1.5
Ca/Al_2O_3	ditto	$Ca(NO_3)_2 \cdot 4\,H_2O$	15	1.5

[a] Loading was calculated in carbonate form.

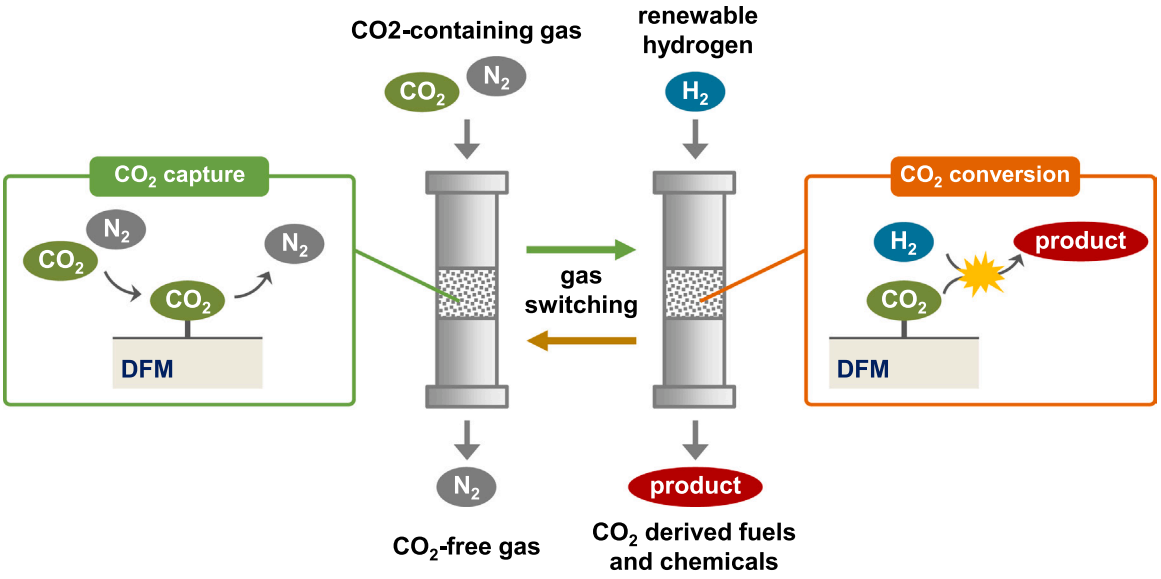

Fig. 1. Conceptual diagram of integrated CO_2 capture and conversion using DFMs.

2.2. Characterization of DFM

The textural properties were analyzed by N_2 adsorption-desorption isotherms at − 196 °C using a surface area and pore size distribution analyzer (BELSORP MAX, Microtrac MRB). The specific surface area was calculated by the Brunauer-Emmett-Teller (BET) method using the adsorption data in the relative pressure (P/P_0) range of 0.05 − 0.25. The pore volume was obtained by accumulating up to $P/P_0 = 0.95$. The pore size distribution was determined by the nonlinear density functional theory (NLDFT) method using desorption branch isotherm. To determine the crystalline structures, powder X-ray diffraction (XRD) was conducted by operating a diffractometer (SmartLab SE, Rigaku Corp.) at 40 keV and 50 mA. A Cu Kα radiation ($\lambda = 1.5418$ Å) was used as an X-ray source. Wide-angle XRD patterns were collected in the 2θ range of 10 − 80° using a step size of 0.02° and a scanning rate of 2 s per step.

The reducibility and surface basicity of the DFMs were studied by H_2 temperature-programmed reduction (H_2-TPR) and CO_2 temperature-programmed desorption (CO_2-TPD) using a catalyst analyzer (BELCAT II, Microtrac MRB) equipped with a thermal conductivity detector (TCD) and a quadrupole mass spectrometer (BELMASS, Microtrac MRB). Prior to H_2-TPR measurement, 0.1 g of sample was loaded in a quartz tube and pre-treated at 50 °C in a 5.05 vol% H_2/Ar stream (15 mL/min) until the TCD signals were stable. The H_2-TPR profiles were recorded at 0–500 °C using a 5.05 vol% H_2/Ar flow (15 mL/min) and a heating rate of 10 °C/min. The signals of H_2, H_2O, CO, and CO_2 were detected by m/z ratios of 2, 18, 28, and 44, respectively. Prior to CO_2-TPD measurement, the sample was reduced by a H_2 flow (50 mL/min) at 500 °C for 1 h, and purged by an Ar flow until the temperature of sample was decreased to 50 °C and the TCD signals were stable at that temperature. The reduced samples were treated by a 5 vol% CO_2/Ar (50 mL/min) at 50 °C for 30 min, and purged by an Ar flow of 50 mL/min to remove physically adsorbed CO_2. The CO_2-TPD profiles were obtained by heating the CO_2-adsorbed sample at 0–800 °C using a heating rate of 10 °C/min and an Ar flow of 30 mL/min.

2.3. CO_2 capture and conversion to CO

Fig. 2 shows a schematic of the experimental apparatus. It consists of mass flow controllers for gas supply, an electric furnace, a stainless-steel reactor (i.d. 9 mm, length 400 mm), a thermoelectric cooler, and a continuous gas analyzer. One gram of DFM was packed in the fixed-bed reactor, and the bed height was approximately 20 mm. Thermocouples covered by a stainless-steel tube was inserted into the reactor to monitor the reaction temperatures at the top, middle, and bottom part of the packed bed. As a pre-treatment to activate the CO_2-capturing capacity of the DFM by decarbonation (reverse of Eq. 1), the packed bed was heated to 500 °C at 10 °C/min in a 100 mL/min flow of H_2 and maintained at that temperature for 1 h.

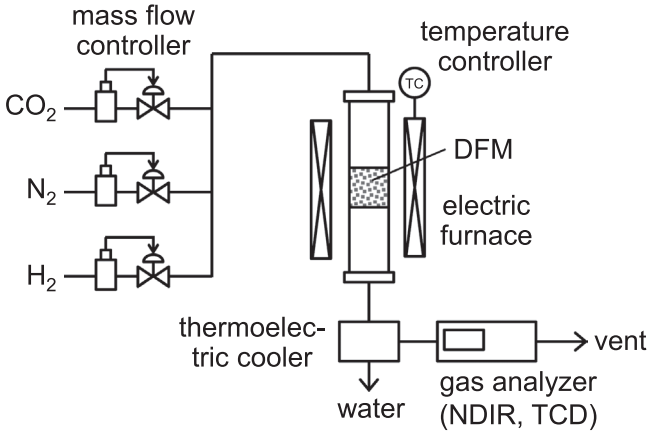

Fig. 2. Schematic diagram of experimental apparatus.

The ICCC experiments were composed of four steps, as listed in Table 2. In step 1, 5 vol% CO_2/N_2 was supplied to the reactor at a flow rate of 500 mL/min for 3 min to capture CO_2. In step 2, the gas stream was switched to N_2 to purge the CO_2. In step 3, H_2 was fed to the reactor at a predetermined flow rate to convert the captured CO_2. Finally, in step 4, N_2 was supplied in the same manner as in step 2 to purge H_2 and the converted products remaining in the reactor. Upon completion of step 4, the experimental operation was repeated from step 1. The reaction temperature was varied in the range of 350–500 °C between runs, although each individual run was isothermal. In addition, the H_2 flow rate in step 3 was regulated in the range of 25–500 mL/min, which corresponds to a weight hourly space velocity (WHSV) of 1.5–30 L/(h·g). During that time, the H_2 supply time was changed to maintain a constant total H_2 input. In each experiment, steps 1–4 were repeated for a minimum of four cycles, and the values observed were expressed as means ± standard deviations. For reference, identical experiments were conducted using γ-Al_2O_3.

In analysis, the moisture in the outlet gas was condensed and removed by the thermoelectric cooler, and the concentrations of CO_2, CO, CH_4, and H_2 were measured using a continuous gas analyzer (Rosemount X-STREAM Enhanced XEGP, Emerson Electric Co.). For quantitative analysis, the amount of CO_2 captured (C_{CO_2}) per unit weight of DFM (W) was calculated by integrating the CO_2 profile during steps 1–2 as follows:

$$C_{CO_2} = \frac{1}{W}\left[\int_{t_0}^{t_1}\left\{F_{CO_{2,f}}(t) - F_{CO_2}(t)\right\}dt - \int_{t_1}^{t_2} F_{CO_2}(t)dt\right] \quad (6)$$

where t_0, t_1, and t_2 represent the time at the start of the experiment, the end of step 1, and the end of step 2, respectively. $F_{CO_{2,f}}$ and F_{CO_2} denote the CO_2 molar flow rates of the feed stream and outlet gas, respectively. In addition, the outflowing amount (n_i) of component i ($i = CO_2$, CO, CH_4) was calculated by integrating the concentration profile during steps 3–4 as follows:

$$n_i = \frac{1}{W}\int_{t_2}^{t_4} F_i(t)dt \quad (7)$$

where t_4 and F_i represent the time at the end of step 4 and the outlet molar flow rate of component i, respectively. From these values, the conversion based on the amount of CO_2 captured (X_{CO_2}), the selectivity for CO (S_{CO}), the yield of CO (Y_{CO}), and the material balance of carbon (B_C) were calculated as follows:

$$X_{CO_2} = \frac{n_{CO} + n_{CH_4}}{C_{CO_2}} \times 100 \quad (8)$$

$$S_{CO} = \frac{n_{CO}}{n_{CO} + n_{CH_4}} \times 100 \quad (9)$$

$$Y_{CO} = \frac{n_{CO}}{C_{CO_2}} \times 100 = \frac{X_{CO_2} S_{CO}}{100} \quad (10)$$

$$B_C = \frac{n_{CO_2} + n_{CO} + n_{CH_4}}{C_{CO_2}} \times 100 \quad (11)$$

Table 2
Experimental conditions for ICCC using 1 g of DFM.

step	supply gas	temperature [°C]	pressure [MPa]	flow rate [mL/min]	time [min]
1	5 vol% CO_2/N_2	350–500	spontaneous (0.1)	500	3
2	N_2	ditto	ditto	500	3
3	H_2	ditto	ditto	25–500	6–120
4	N_2	ditto	ditto	500	3

2.4. Syngas production from atmospheric-level CO_2

To enrich the CO concentration, scale-up experiments were performed. Sixty grams of the DFM was packed in a fixed bed reactor (i.d. 25 mm, length 400 mm) made of stainless steel, and the bed height was approximately 250 mm. In a 500 mL/min flow of H_2, the packed bed was heated at 10 °C/min up to 500 °C and maintained thereat for 2 h. Although the ICCC experiments were performed using the procedure described in Section 2.3, step 4 was omitted because the experiments were not cyclically repeated. The experimental conditions for steps 1–3 are listed in Table 3. The changes were that the CO_2 feed concentration in step 1 was set at 5 vol% or 400 ppm, and the gas flow rates of all the steps were arbitrarily doubled because a high flow rate would be required to maintain the WHSV employed in the 1 g-DFM experiments. The H_2 flow rate in step 3 was experimentally optimized as described in the following section.

In analysis, a dual-channel micro gas chromatograph (GC) equipped with TCDs (Agilent 490, Agilent Technologies, Inc.) was used in addition to the continuous gas analyzer. The analytical method with the micro-GC is described below. The exhaust gas from the continuous gas analyzer was collected in a gas bag for analysis during step 3. In channel 1 of the micro-GC, a Molsieve 5 Å column(Agilent Technologies, Inc.) was used to measure the concentrations of H_2, CO, and CH_4. Ar was used as the carrier gas, and the column temperature and pressure were 100 °C and 170 kPa, respectively. In channel 2, a PoraPLOT Q column (Agilent Technologies, Inc.) was used to determine the concentration of CO_2. He was used as the carrier gas, and the column temperature and pressure were 80 °C and 170 kPa, respectively.

3. Results and discussion

3.1. Characterization of DFM

The results of the characterization are shown in the Supplementary Materials and are briefly described in this section. Table S1 shows the textural properties of the as-prepared DFMs as measured by N_2 adsorption-desorption analysis. Compared to the bare alumina support, the DFMs prepared using alkali or alkaline earth metals exhibited smaller BET surface areas and pore volumes, although the pore sizes were nearly identical. This result suggests that DFMs maintain appropriate porous structures. The crystalline structures were analyzed using XRD, as shown in Fig. S1. Small diffraction peaks attributed to the corresponding alkali carbonate were detected in addition to the γ-Al_2O_3 peaks in the XRD patterns of Na/Al_2O_3 and K/Al_2O_3. In contrast, only γ-Al_2O_3 peaks were detected in the XRD pattern of Ca/Al_2O_3. This result indicates that alkali or alkaline earth metals are uniformly dispersed on the alumina support.

Fig. S2 shows the H_2-TPR profiles of the DFM samples. All the samples underwent the desorption of H_2O in the range of 50–300 °C. For the DFMs, trace amounts of CO_2 and CO were detected at temperatures exceeding 400 °C. They were not detected when using the bare alumina support. This result implies that the release of CO_2 by decarbonation (reverse of Eq. 1) and the conversion of CO_2 to CO (Eq. 3) occur when using the DFMs. Fig. S3 shows the CO_2-TPD profiles of the DFMs. For all the samples, a broad CO_2 peak appeared at approximately 100 °C, which indicates the desorption of weakly adsorbed CO_2. The DFMs prepared using alkali or alkaline earth metals have higher basicity than the bare alumina support and consequently exhibit a more intense CO_2 peak. An additional CO_2 peak that was attributed to decarbonation was observed at temperatures exceeding 600 °C. CO_2-TPD conducted in an inert atmosphere required a high temperature for decarbonation compared to H_2-TPR conducted in a reducing atmosphere.

Table 3
Experimental conditions for ICCC using 60 g of DFM.

step	supply gas	temperature [°C]	pressure [MPa]	flow rate [mL/min]	time [min]
1	5 vol%, 400 ppm CO_2/N_2	500	spontaneous (0.1)	1000	15, 720
2	N_2	ditto	ditto	1000	15
3	H_2	ditto	ditto	200	60

3.2. Screening of supported alkali/alkaline-earth metals

Fig. 3 shows the concentration profiles plotted during the ICCC experiments using the prepared DFMs at 450 °C and an H_2 flow rate of 100 mL/min. The effluent gas volume and time elapsed since the start of step 1 are both plotted along the horizontal axes. The time scale for step 3 is different from that for the other steps because of the lower flow rate. As shown in Fig. 3(a), when using Na/Al_2O_3, CO_2 was not detected immediately upon commencing the CO_2 supply in step 1, which means that CO_2 was aggressively captured in the DFM during the initial period. Following the breakthrough, the CO_2 concentration increased rapidly and approached the feed concentration. While purging CO_2 using N_2 in step 2, the CO_2 concentration decreased rapidly. Immediately upon the commencement of H_2 supply in step 3, the CO concentration increased rapidly, and gradually decreased after reaching the maximum. At the end of step 4, the H_2 concentration was confirmed to fall below 0.5 vol% (data not shown).

Similar gas responses were observed from K/Al_2O_3, as shown in Fig. 3(b). As shown in Fig. 3(c), the CO peak produced in step 3 was lower when using Ca/Al_2O_3. Finally, as shown in Fig. 3(d), the breakthrough in step 1 when using the reference alumina occurred earlier than that for the DFMs, and a small amount of CO was detected in step 3. These results indicate that the transition-metal-free DFMs developed in this study facilitate rapid conversion of CO_2 into CO at a lower temperature than previously reported CaO-based ICCCs [18,29].

For quantitative discussion, the amounts of CO_2 captured and outflow of each component during steps 3–4 are shown in Fig. 4. The amount of CO_2 captured decreased in the following order: $K/Al_2O_3 > Na/Al_2O_3 > Ca/Al_2O_3 > Al_2O_3$, which indicates that alkali or alkaline earth metals play an important role in CO_2 capture. For all the DFMs, the majority of the captured CO_2 was converted into CO, and the amount of CO produced was of the same order as the amount of CO_2 captured. In addition, the released amount of unreacted CO_2 was small. From these results, we infer that the direct synthesis of CO may proceed from alkali or alkaline earth carbonates (Eq. 12) through an overall reaction of decarbonation (reverse of Eq. 1) and the RWGS (Eq. 3).

$$M_xCO_3 + H_2 \rightleftharpoons M_xO + CO + H_2O \quad (12)$$

Additionally, a trace amount of CH_4 was also produced. There are two possible reaction pathways for CH_4 formation: (i) parallel formation with CO by the Sabatier reaction (Eq. 2) and (ii) sequential formation from CO by methanation (Eq. 13).

$$CO + 3\,H_2 \rightleftharpoons CH_4 + H_2O \quad (13)$$

The conversions of captured CO_2, selectivities for CO, CO yields, and carbon material balances achieved by the DFMs are compared in Table 4. The highest conversion of 90.2% was obtained using Na/Al_2O_3. The CO selectivity of all the DFMs exceeded 90%, with Na/Al_2O_3 achieving the highest selectivity. The CO yield of Na/Al_2O_3 was the highest because of its well-balanced ICCC performance. The carbon material balance was approximately 90–95% for all the DFMs, which indicates that nearly all of the captured CO_2 was released as CO_2, CO, or CH_4.

In summary, the transition-metal-free DFMs prepared herein using alkali or alkaline earth metals facilitated the capture of CO_2 and its selective conversion into CO. Although the amounts of CO_2 captured and CO produced were highest for K/Al_2O_3, the CO yield was the highest for

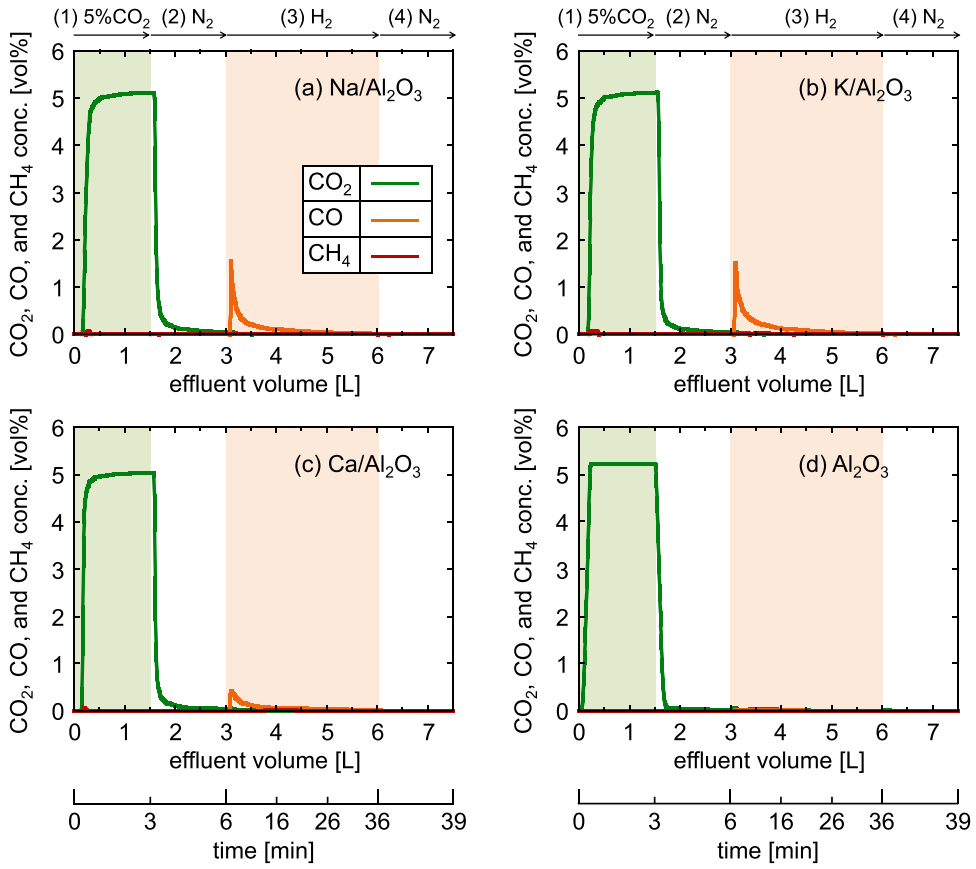

Fig. 3. Concentration profiles during integrated CO_2 capture and conversion with (a) Na/Al_2O_3, (b) K/Al_2O_3, (c) Ca/Al_2O_3, and (d) Al_2O_3 at 450 °C and an H_2 flow rate of 100 mL/min.

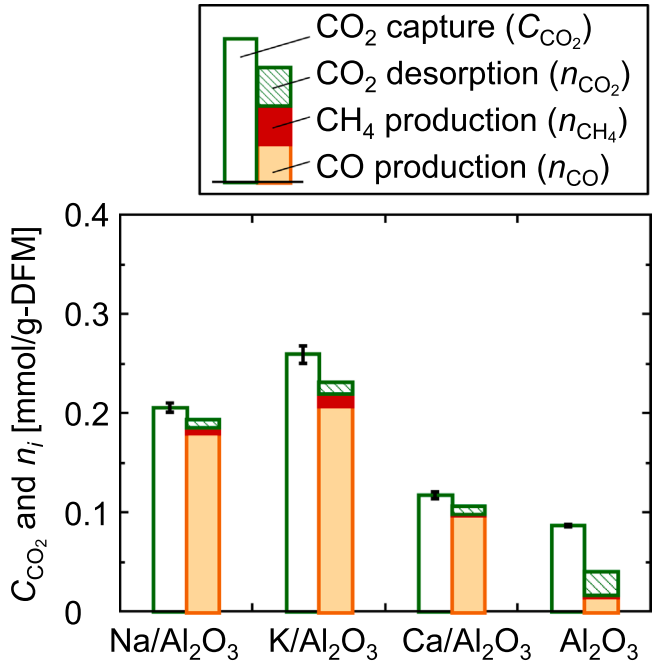

Fig. 4. CO_2 capture and conversion performance of the prepared DFMs at 450 °C and an H_2 flow rate of 100 mL/min.

Table 4
Comparison of the conversion of captured CO_2 (X_{CO_2}), selectivity for CO (S_{CO}), CO yield (Y_{CO}), and carbon material balance (B_C) achieved by the prepared DFMs.

sample	X_{CO_2} [%]	S_{CO} [%]	Y_{CO} [%]	B_C [%]
Na/Al_2O_3	90.2 ± 1.8	96.9 ± 0.3	87.4 ± 2.0	94.6 ± 1.9
K/Al_2O_3	85.0 ± 2.7	93.9 ± 0.7	79.8 ± 1.9	89.4 ± 2.8
Ca/Al_2O_3	86.2 ± 3.7	96.0 ± 1.9	82.7 ± 2.6	93.6 ± 4.1
Al_2O_3	20.3 ± 0.2	89.6 ± 0.3	18.1 ± 0.2	47.1 ± 0.6

Na/Al_2O_3. Hence in subsequent experiments, the Na/Al_2O_3 DFM was employed.

3.3. Effect of reaction temperature and H_2 flow rate on integrated CO_2 capture and reduction

Fig. 5 shows the experimental results when Na/Al_2O_3 was used as the DFM and the reaction temperature was varied in the range of 350–500 °C. During this investigation, the H_2 flow rate in step 3 was set at 100 mL/min, as described in the previous section. The CO production peak in step 3 increased in intensity as the reaction temperature increased. The amount of CO_2 captured, conversion of captured CO_2, and selectivity for CO are summarized in Fig. 6. The amount of CO_2 captured, shown using a bar chart is higher at lower temperatures. This occurred because CO_2 capture by carbonation (Eq. 1) is exothermic, and lower temperatures are thermodynamically favorable. The CO_2 conversion, shown as a square symbol, drastically increased with temperature, and the values at 450 and 500 °C were almost identical at approximately 90%. The CO selectivity (shown as the circle symbol) exceeded 95% in the temperature range of 350–500 °C. However, it

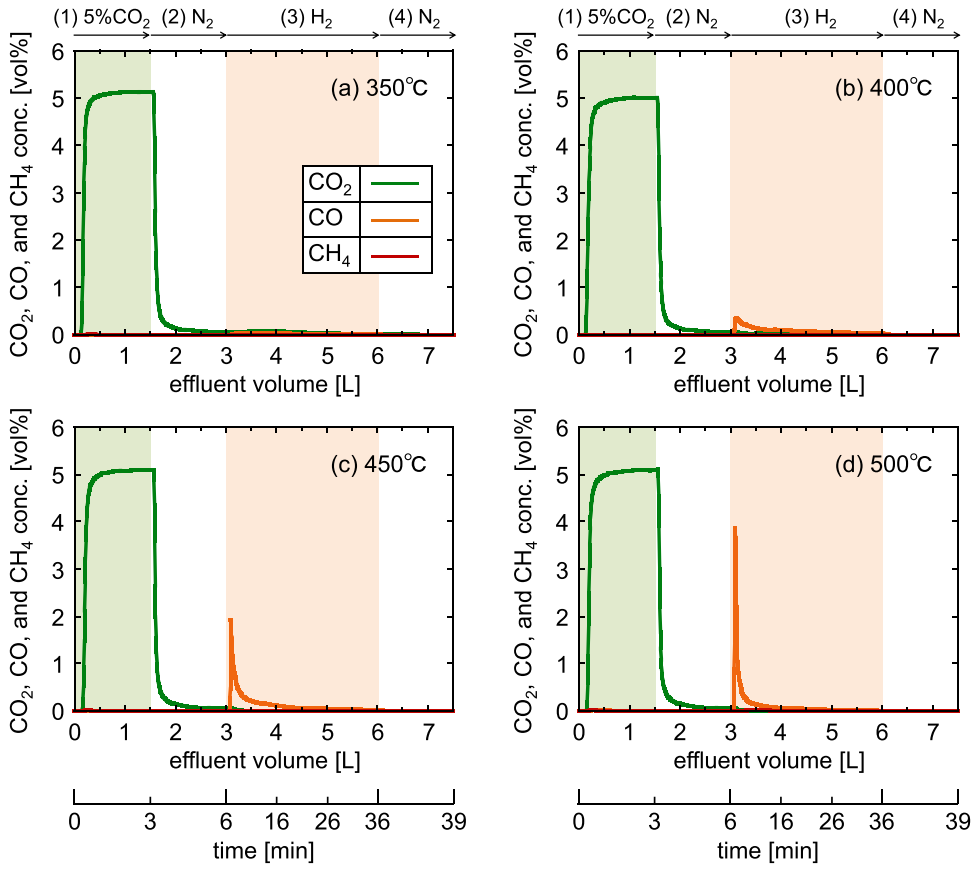

Fig. 5. Concentration profiles during integrated CO_2 capture and conversion using Na/Al_2O_3 at 350–500 °C and an H_2 flow rate of 100 mL/min.

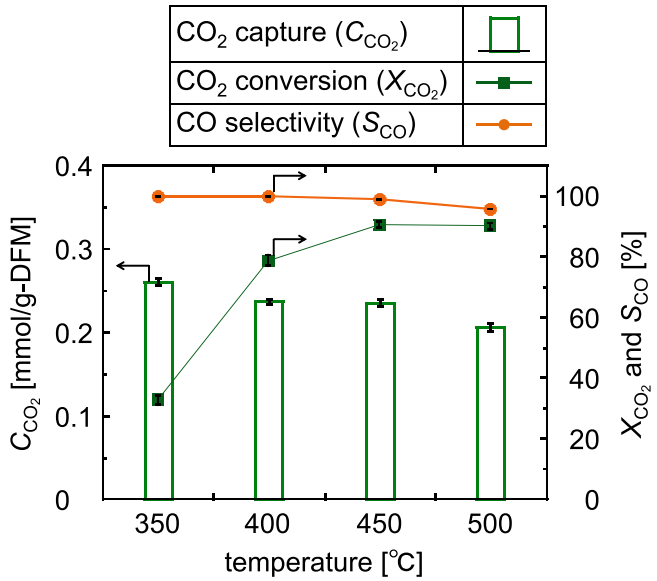

Fig. 6. Effect of reaction temperature on amount of CO_2 captured, CO_2 conversion, and CO selectivity using Na/Al_2O_3 at an H_2 flow rate of 100 mL/min.

decreased slightly at higher temperatures.

Furthermore, the effects of H_2 flow rates in step 3 were studied at 450 °C as shown in Fig. 7. The maximum CO concentration increased as the H_2 flow rate decreased. A similar trend was observed at other temperatures (data not shown). The conversion of captured CO_2 and selectivity for CO were calculated from the concentration profiles in Fig. 7, and are summarized in Fig. 8 with the results obtained at different temperatures. The H_2 flow rate and the corresponding WHSV are plotted along the horizontal axes. Comparing the results generated at identical H_2 flow rates in Fig. 8(a), higher temperatures evidently resulted in higher CO_2 conversions, although there was no significant difference between the values at 450 and 500 °C. The main reaction, namely the production of CO by the RWGS reaction (Eq. 3), is endothermic. Consequently, higher temperatures are favorable in terms of thermodynamics and kinetics. Comparing the results generated under identical temperatures, a lower flow rate, that is, a longer residence time, resulted in a higher conversion. As shown in Fig. 8(b), the CO selectivity decreased marginally with increase in the temperature and decrease in the H_2 flow rate. The decrease in the CO selectivity indicates a higher proportion of CH_4 in the product. Both the CH_4 formation reactions (Eq. 2, Eq. 13) are exothermic; therefore, they are thermodynamically unfavorable at high temperatures. This suggests that the formation of CH_4 is kinetically limited in this system. Therefore, the CH_4 formation with a low reaction rate proceeds at a lower H_2 flow rate, that is, a longer residence time, resulting in the slight decrease in the CO selectivity.

In summary, a higher reaction temperature slightly reduced the amount of CO_2 captured and the selectivity toward CO, but significantly improved the conversion of captured CO_2. Therefore, a reaction temperature of 450–500 °C was found to be preferable for ICCC to CO using the transition-metal-free DFM. Reducing the flow rate of H_2 increased the conversion but slightly reduced the CO selectivity. An H_2 flow rate of approximately 100 mL/min, that is, a WHSV of 6 L/(g·h), was found to be optimal. Under the optimized conditions, the conversion and selectivity exceeded 90% and 95%, respectively.

3.4. Stability of DFM

Fig. 9 shows the transitions of the amounts of captured CO_2 and produced CO during 50 cycles of ICCC using the Na/Al_2O_3 DFM. The

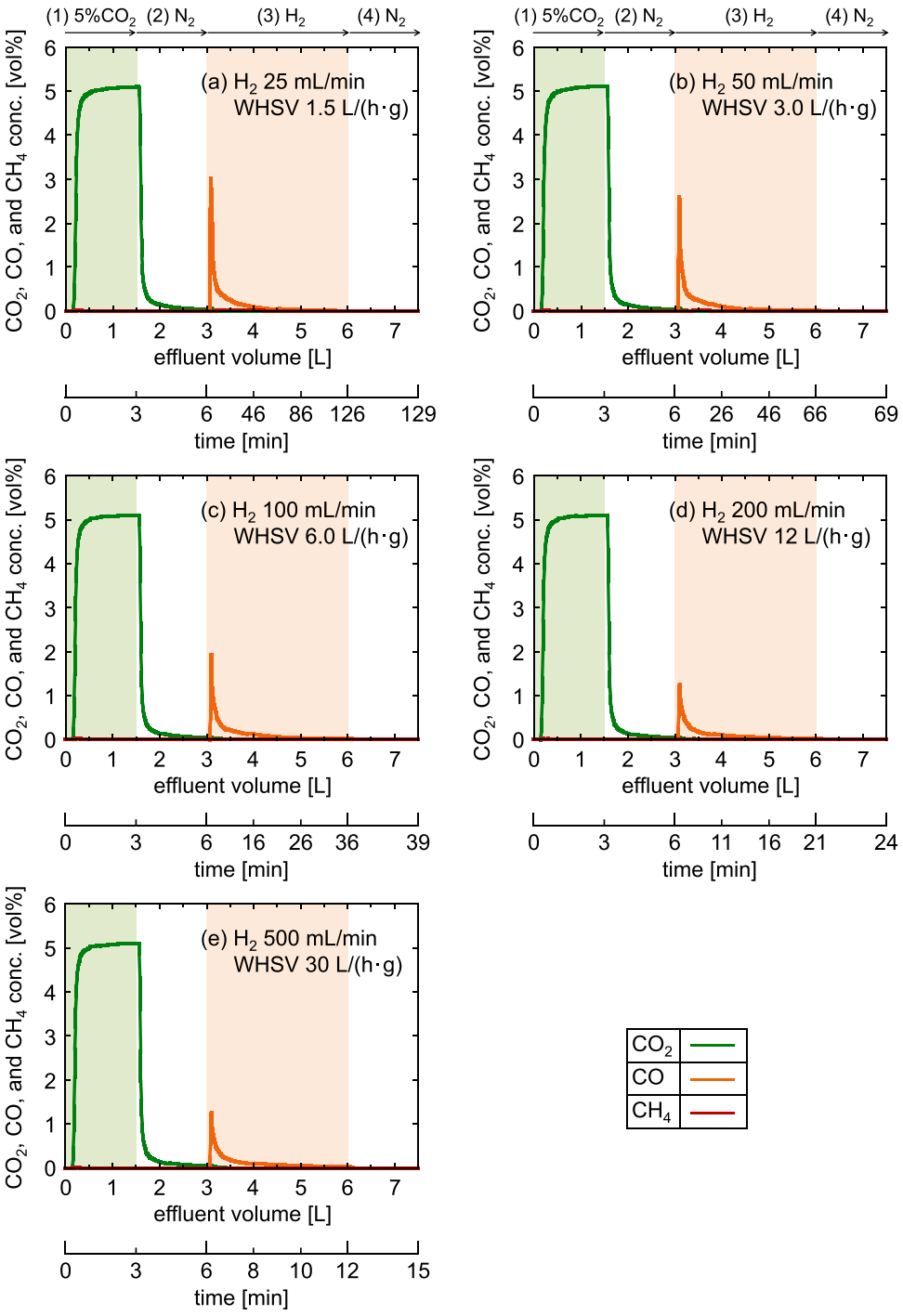

Fig. 7. Concentration profiles during ICCC using Na/Al_2O_3 at 450 °C and an H_2 flow rate of 25–500 mL/min.

reaction temperature was 450 °C, and the H_2 flow rate was 100 mL/min. In the second cycle, the amount of CO_2 captured decreased to approximately 80% of that in the first cycle. Thereafter, this value remained nearly constant. The amount of CO_2 captured in the first cycle was particularly high because the pre-treatment of DFM was conducted at 500 °C, which was higher than the reaction temperature of the ICCC experiments (450 °C). Decarbonation (reverse of Eq. 1) would proceed more efficiently during the pre-treatment than during step 3 for CO_2 conversion in each cycle. The amount of CO produced did not change significantly during the 50 cycles. As mentioned in Section 3.2, Na/Al_2O_3 achieved a high carbon material balance of approximately 95%; consequently, no carbon was accumulated during the cycles, resulting in high stability.

The textural properties and crystalline structures of as-prepared and used Na/Al_2O_3 DFM were compared. As shown in the aforementioned Table S1, the textural properties of used Na/Al_2O_3 such as the BET surface areas, pore volumes, and pore sizes were nearly identical to those of as-prepared Na/Al_2O_3. The crystalline structures analyzed using XRD are shown in Fig. S4. A significant difference was not observed between as-prepared and used Na/Al_2O_3. In summary, these findings demonstrate the reusability of the Na/Al_2O_3 DFM for repetitive ICCC to CO without significant deactivation.

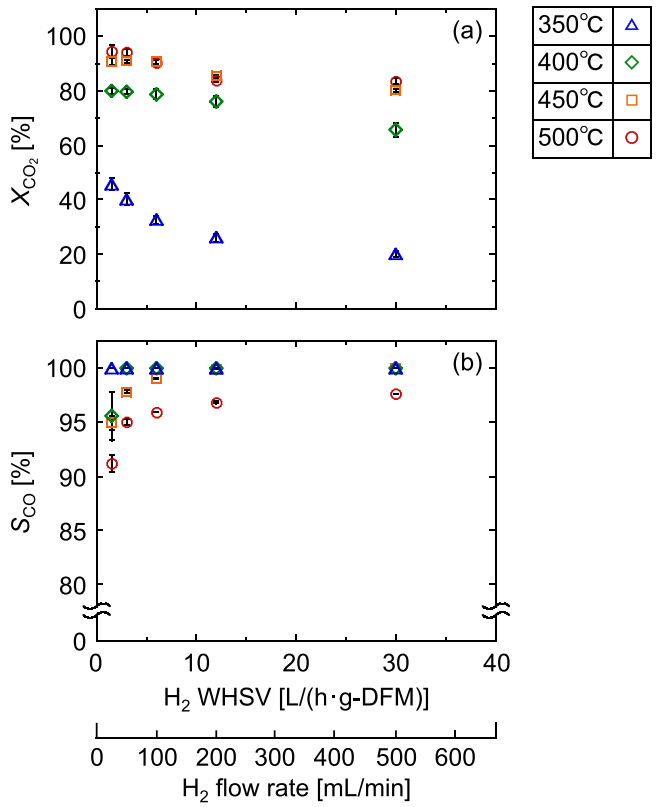

Fig. 8. Effect of H_2 flow rate and reaction temperature on (a) CO_2 conversion and (b) CO selectivity of Na/Al_2O_3.

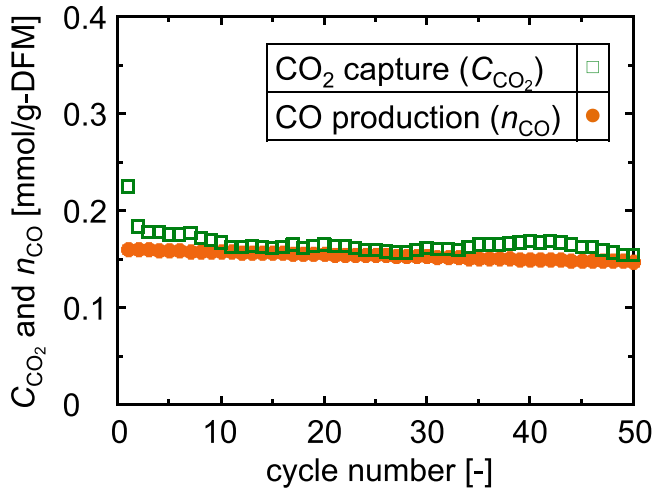

Fig. 9. Transitions of the amounts of CO_2 captured and CO produced during the 50-cycle stability test at 450 °C.

3.5. Syngas production from atmospheric-level CO_2

In this section, the scale-up ICCC experiments with 5 vol% and 400 ppm CO_2 were performed to verify a production of syngas with a practical H_2/CO ratio. Fig. 10 shows the concentration profiles using 5 vol% CO_2 and 60 g of Na/Al_2O_3 DFM, which was 60 times larger scale than the previous experiments. Fig. 10(a) and (b) show the results of steps 1–3 (CO_2 capture, purging using N_2, and CO_2 conversion, respectively). The time span depicted in each figure is different. The vertical axes are common in Fig. 10(a) and (b). Fig. 10(c) is an enlarged view of the initial 3 min of step 3, and the concentrations of CO_2, CO, CH_4, and

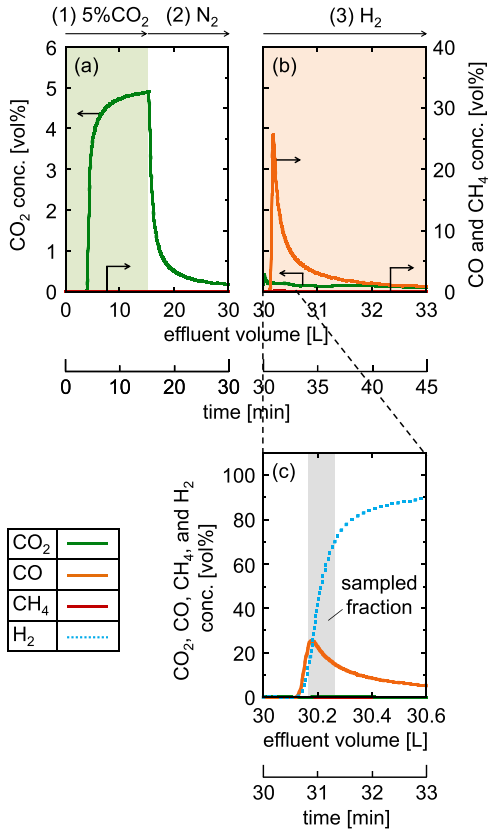

Fig. 10. Concentration profiles recorded during (a) the CO_2-capturing step for 5 vol% CO_2 and (b, c) the conversion step using 60 g of Na/Al_2O_3 at 500 °C.

H_2 are shown on the same scale. As shown in Fig. 10(a), in step 1, the CO_2 concentration was lower than 0.1 ppm until approximately 4 min, whereafter it rapidly increased to the feed concentration. During step 2, the CO_2 concentration decreased rapidly. As shown in Fig. 10(b) and (c), the formation of CO was observed immediately upon commencement of step 3. The CO concentration reached a very high value of 25 vol% at the maximum, and the corresponding CO_2 concentration was surprisingly low, less than 0.5 vol%. Simultaneously, the concentration of H_2 increased and finally approached 100 vol%.

Furthermore, we also challenged the direct syngas production from very dilute CO_2 at the atmospheric level (400 ppm) as shown in Fig. 11. As expected, a significantly longer time elapsed until the breakthrough in step 1 owing to the lower feed concentration of CO_2 (Fig. 11(a)). In step 2, the CO_2 concentration did not decreased from the value at the end of step 1. Because of the very dilute feed concentration of CO_2, a slight CO_2 release from the DFM in an inert N_2 atmosphere was remarkably observed. As shown in Fig. 11(b) and (c), the maximum CO concentration exceeded 20 vol% even from 400 ppm CO_2. This result indicates that Na/Al_2O_3 DFM can directly convert and enrich atmospheric level CO_2 into CO with more than 500 times higher concentration.

For quantitative analysis, the outlet gas fractions in the vicinity of the CO peak that are indicated by the gray-shaded area in Fig. 10(c) and Fig. 11(c) were collected to analyze the composition by micro-GC. The analysis results of CO_2, CO, CH_4, and H_2 are summarized in Table 5. When the feed concentration of CO_2 in step 1 was 5 vol%, the concentrations of CO and unreacted H_2 in step 3 were 19.7 and 55.9 vol%, respectively. Therefore, the H_2/CO ratio was 2.8, which is practically feasible for the Fischer-Tropsch synthesis (Eq. 5). In addition, similar to the experimental results with 1 g-DFM described above, the amounts of unreacted CO_2 and produced CH_4 were negligible. When using 400 ppm CO_2, even though the feed concentration of CO_2 was two orders of

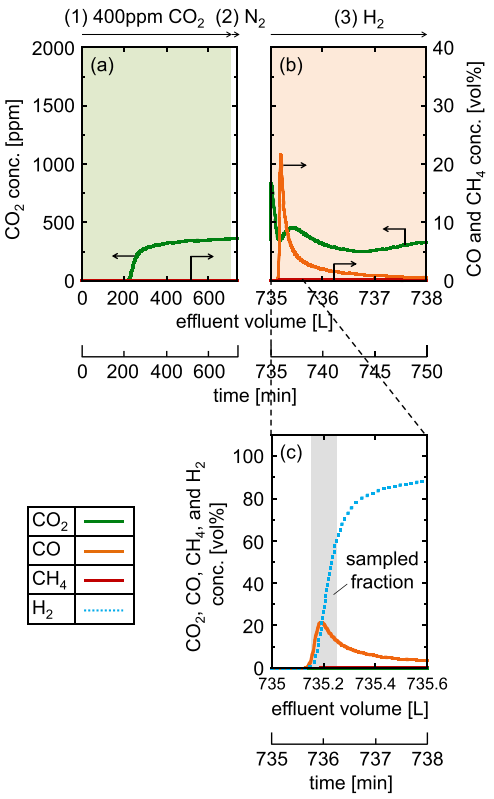

Fig. 11. Concentration profiles during (a) the CO_2-capture step using 400 ppm CO_2 and (b, c) the conversion step using 60 g of Na/Al_2O_3 at 500 °C.

Table 5
Compositions of fractions collected during the conversion step following the capture step for 5 vol% and 400 ppm CO_2.

component [vol%]	5 vol% CO_2	400 ppm CO_2
CO_2	0.294	0.0558
CO	19.7	14.5
CH_4	0.363	1.31
H_2	55.9	48.1

magnitude lower than that when using 5 vol% CO_2, a high CO concentration of 14.5 vol% was obtained. A slight decrease in the CO production resulted from the smaller amount of captured CO_2. A near-practical H_2/CO ratio of 3.3 was also achieved using 400 ppm CO_2.

Table S2 in the Supplementary Materials shows the amount of CO_2 captured, conversion of captured CO_2, and selectivity for CO. Although the CO selectivity was similar to the experimental results obtained using 1 g-DFM at 500 °C, the amount of CO_2 captured and the conversion decreased. This occurred mainly because the bed height when using 60 g-DFM was approximately 250 mm, and there was an axial temperature distribution (Figs. S5 and S6). This is not a shortcoming of the DFM and can be improved by constructing an appropriately scaled experimental apparatus.

So far, only a pioneer work of Hu and Wang's research group has reported the scale-up ICCC to CO using DFMs [28]. They demonstrated that 25 g of $Fe_5Co_5Mg_{10}CaO$ DFM produced CO with the maximum concentration of approximately 15 vol% at 650 °C following CO_2 capture using a simulated flue gas containing 10 vol% CO_2. An H_2/CO ratio was not mentioned in the work. The transition-metal-free Na/Al_2O_3 DFM prepared herein demonstrated the potential to directly produce syngas with a near-practical H_2/CO even from atmospheric-level CO_2 at a lower reaction temperature.

4. Conclusion

In this study, ICCC experiments were performed to synthesize CO by employing transition-metal-free DFMs prepared by impregnation of alkali or alkaline earth metals on γ-Al_2O_3. During the screening of the DFMs prepared, although the capacity of Na/Al_2O_3 for CO_2 capture was slightly lower than that of K/Al_2O_3, Na/Al_2O_3 was selected because it exhibited the highest yield of CO. The effect of the operating conditions on CO_2 capture and conversion using Na/Al_2O_3 DFM was investigated. Although increasing the reaction temperature slightly reduced the amount of CO_2 captured and the selectivity for CO, it significantly improved the conversion of captured CO_2. Reducing the flow rate of H_2 increased the conversion, but marginally decreased the CO selectivity. The optimized conditions were a reaction temperature of 450–500 °C and an H_2 WHSV of 6 L/(g·h), under which the conversion and selectivity exceeded 90% and 95%, respectively. A 50-cycles stability test revealed that the Na/Al_2O_3 DFM is reusable for repetitive ICCC to CO without significant deactivation. Finally, the scale-up experiments demonstrated that the transition-metal-free DFM has the potential to directly produce syngas from atmospheric-level CO_2, which leads to further conversion into value-added products such as fuels and chemicals. In conclusion, ICCC using the transition-metal-free DFM developed in this study may be practicable provided the CO_2 capture capacity of the DFM is further improved while maintaining the aforementioned advantages. For that purpose, mechanistic in situ and operando studies for revealing the state of the active Na species need to be performed in the future. Further investigations with realistic flue gas containing impurities such as O_2 and H_2O are also important to verify the practical availability of the DFMs.

CRediT authorship contribution statement

Tomone Sasayama: Methodology, Investigation, Formal analysis, Visualization, Writing – original draft **Fumihiko Kosaka:** Methodology, Investigation, Writing – review & editing, Supervision **Yanyong Liu:** Conceptualization **Toshiaki Yamaguchi:** Conceptualization **Shih-Yuan Chen:** Investigation, Visualization, Writing – review & editing **Takehisa Mochizuki:** Methodology, Conceptualization **Atsushi Urakawa:** Writing – review & editing, Validation, Supervision **Koji Kuramoto:** Writing – review & editing, Project administration.

Declaration of Competing Interest

The authors declare that they have no known competing financial interests or personal relationships that could have appeared to influence the work reported in this paper.

Acknowledgements

This research did not receive any specific grant from funding agencies in the public, commercial, or not-for-profit sectors.

Appendix A. Supporting information

Supplementary data associated with this article can be found in the online version at doi:10.1016/j.jcou.2022.102049.

References

[1] K.M.K. Yu, I. Curcic, J. Gabriel, S.C.E. Tsang, Recent advances in CO_2 capture and utilization, ChemSusChem 1 (2008) 893–899, https://doi.org/10.1002/cssc.200800169.
[2] M. Peters, B. Köhler, W. Kuckshinrichs, W. Leitner, P. Markewitz, T.E. Müller, Chemical technologies for exploiting and recycling carbon dioxide into the value chain, ChemSusChem 4 (2011) 1216–1240, https://doi.org/10.1002/cssc.201000447.

[3] Z. Yuan, M.R. Eden, R. Gani, Toward the development and deployment of large-scale carbon dioxide capture and conversion processes, Ind. Eng. Chem. Res. 55 (2016) 3383–3419, https://doi.org/10.1021/acs.iecr.5b03277.
[4] R.S. Norhasyima, T.M.I. Mahlia, Advances in CO_2 utilization technology: a patent landscape review, J. CO2 Util. 26 (2018) 323–335, https://doi.org/10.1016/j.jcou.2018.05.022.
[5] T.A. Atsbha, T. Yoon, P. Seongho, C.-J. Lee, A review on the catalytic conversion of CO_2 using H2 for synthesis of CO, methanol, and hydrocarbons, J. CO2 Util. 44 (2021), 101413, https://doi.org/10.1016/j.jcou.2020.101413.
[6] S. Saeidi, S. Najari, V. Hessel, K. Wilson, F.J. Keil, P. Concepción, S.L. Suib, A. E. Rodrigues, Recent advances in CO_2 hydrogenation to value-added products — current challenges and future directions, Prog. Energy Combust. Sci. 85 (2021), 100905, https://doi.org/10.1016/j.pecs.2021.100905.
[7] M. Bui, C.S. Adjiman, A. Bardow, E.J. Anthony, A. Boston, S. Brown, P.S. Fennell, S. Fuss, A. Galindo, L.A. Hackett, J.P. Hallett, H.J. Herzog, G. Jackson, J. Kemper, S. Krevor, G.C. Maitland, M. Matuszewski, I.S. Metcalfe, C. Petit, G. Puxty, J. Reimer, D.M. Reiner, E.S. Rubin, S.A. Scott, N. Shah, B. Smit, J.P.M. Trusler, P. Webley, J. Wilcox, N.M. Dowell, Carbon capture and storage (CCS): the way forward, Energy Environ. Sci. 11 (2018) 1062–1176, https://doi.org/10.1039/C7EE02342A.
[8] R.M. Cuéllar-Franca, A. Azapagic, Carbon capture, storage and utilisation technologies: a critical analysis and comparison of their life cycle environmental impacts, J. CO2 Util. 9 (2015) 82–102, https://doi.org/10.1016/j.jcou.2014.12.001.
[9] P. Melo Bravo, D.P. Debecker, Combining CO_2 capture and catalytic conversion to methane, Waste Dispos. Sustain. Energy 1 (2019) 53–65, https://doi.org/10.1007/s42768-019-00004-0.
[10] I.S. Omodolor, H.O. Otor, J.A. Andonegui, B.J. Allen, A.C. Alba-Rubio, Dual-function materials for CO_2 capture and conversion: a review, Ind. Eng. Chem. Res. 59 (2020) 17612–17631, https://doi.org/10.1021/acs.iecr.0c02218.
[11] B. Shao, Y. Zhang, Z. Sun, J. Li, Z. Gao, Z. Xie, J. Hu, H. Liu, CO_2 capture and in-situ conversion: recent progresses and perspectives, Green, Chem. Eng. (2021), https://doi.org/10.1016/j.gce.2021.11.009.
[12] S. Sun, H. Sun, P.T. Williams, C. Wu, Recent advances in integrated CO_2 capture and utilization: a review, Sustain. Energy Fuels 5 (2021) 4546–4559, https://doi.org/10.1039/D1SE00797A.
[13] M.S. Duyar, M.A.A. Treviño, R.J. Farrauto, Dual function materials for CO_2 capture and conversion using renewable H2, Appl. Catal. B 168 169 (2015) 370–376, https://doi.org/10.1016/j.apcatb.2014.12.025.
[14] L. Hu, A. Urakawa, Continuous CO_2 capture and reduction in one process: CO_2 methanation over unpromoted and promoted Ni/ZrO2, J. CO2 Util. 25 (2018) 323–329, https://doi.org/10.1016/j.jcou.2018.03.013.
[15] A. Bermejo-López, B. Pereda-Ayo, J.A. González-Marcos, J.R. González-Velasco, Ni loading effects on dual function materials for capture and in-situ conversion of CO_2 to CH4 using CaO or Na2CO3, J. CO2 Util. 34 (2019) 576–587, https://doi.org/10.1016/j.jcou.2019.08.011.
[16] F. Kosaka, Y. Liu, S.-Y. Chen, T. Mochizuki, H. Takagi, A. Urakawa, K. Kuramoto, Enhanced activity of integrated CO_2 capture and reduction to CH4 under pressurized conditions toward atmospheric CO_2 utilization, ACS Sustain. Chem. Eng. 9 (2021) 3452–3463, https://doi.org/10.1021/acssuschemeng.0c07162.
[17] S.B. Jo, J.H. Woo, J.H. Lee, T.Y. Kim, H.I. Kang, S.C. Lee, J.C. Kim, A novel integrated CO_2 capture and direct methanation process using Ni/CaO catal-sorbents, Sustain. Energy Fuels 4 (2020) 4679–4687, https://doi.org/10.1039/D0SE00760A.
[18] X. Ma, X. Li, H. Cui, W. Zhang, Z. Cheng, Z. Zhou, Metal oxide-doped Ni/CaO dual-function materials for integrated CO_2 capture and conversion: performance and mechanism, AIChE J. (2021), e17520, https://doi.org/10.1002/aic.17520.
[19] L. Proaño, E. Tello, M.A. Arellano-Trevino, S. Wang, R.J. Farrauto, M. Cobo, In-situ DRIFTS study of two-step CO_2 capture and catalytic methanation over Ru,"Na2O"/Al2O3 Dual Functional Material, Appl. Surf. Sci. 479 (2019) 25–30, https://doi.org/10.1016/j.apsusc.2019.01.281.
[20] H. Sun, Y. Zhang, S. Guan, J. Huang, C. Wu, Direct and highly selective conversion of captured CO_2 into methane through integrated carbon capture and utilization over dual functional materials, J. CO2 Util. 38 (2020) 262–272, https://doi.org/10.1016/j.jcou.2020.02.001.
[21] L. Proaño, M.A. Arellano-Treviño, R.J. Farrauto, M. Figueredo, C. Jeong-Potter, M. Cobo, Mechanistic assessment of dual function materials, composed of Ru-Ni, Na2O/Al2O3 and Pt-Ni, Na2O/Al2O3, for CO_2 capture and methanation by in-situ DRIFTS, Appl. Surf. Sci. 533 (2020), 147469, https://doi.org/10.1016/j.apsusc.2020.147469.
[22] A. Bermejo-López, B. Pereda-Ayo, J.A. González-Marcos, J.R. González-Velasco, Modeling the CO_2 capture and in situ conversion to CH4 on dual function Ru-Na2CO3/Al2O3 catalyst, J. CO2 Util. 42 (2020), 101351, https://doi.org/10.1016/j.jcou.2020.101351.
[23] A. Bermejo-López, B. Pereda-Ayo, J.A. González-Marcos, J.R. González-Velasco, Simulation-based optimization of cycle timing for CO_2 capture and hydrogenation with dual function catalyst, Catal. Today (2021), https://doi.org/10.1016/j.cattod.2021.08.023.
[24] L.F. Bobadilla, J.M. Riesco-García, G. Penelás-Pérez, A. Urakawa, Enabling continuous capture and catalytic conversion of flue gas CO_2 to syngas in one process, J. CO2 Util. 14 (2016) 106–111, https://doi.org/10.1016/j.jcou.2016.04.003.
[25] T. Hyakutake, W. van Beek, A. Urakawa, Unravelling the nature, evolution and spatial gradients of active species and active sites in the catalyst bed of unpromoted and K/Ba-promoted Cu/Al2O3 during CO_2 capture-reduction, J. Mater. Chem. A 4 (2016) 6878–6885, https://doi.org/10.1039/C5TA09461E.
[26] H. Sun, J. Wang, J. Zhao, B. Shen, J. Shi, J. Huang, C. Wu, Dual functional catalytic materials of Ni over Ce-modified CaO sorbents for integrated CO_2 capture and conversion, Appl. Catal. B 244 (2019) 63–75, https://doi.org/10.1016/j.apcatb.2018.11.040.
[27] S.B. Jo, J.H. Woo, J.H. Lee, T.Y. Kim, H.I. Kang, S.C. Lee, J.C. Kim, CO_2 green technologies in CO_2 capture and direct utilization processes: methanation, reverse water-gas shift, and dry reforming of methane, Sustain. Energy Fuels 4 (2020) 5543–5549, https://doi.org/10.1039/D0SE00951B.
[28] B. Shao, G. Hu, K.A.M. Alkebsi, G. Ye, X. Lin, W. Du, J. Hu, M. Wang, H. Liu, F. Qian, Heterojunction-redox catalysts of FexCoyMg10CaO for high-temperature CO_2 capture and in situ conversion in the context of green manufacturing, Energy Environ. Sci. 14 (2021) 2291–2301, https://doi.org/10.1039/D0EE03320K.
[29] S. Sun, Z. Lv, Y. Qiao, C. Qin, S. Xu, C. Wu, Integrated CO_2 capture and utilization with CaO-alone for high purity syngas production, Carbon Capture Sci. Technol. 1 (2021), 100001, https://doi.org/10.1016/j.ccst.2021.100001.
[30] G. Wang, Y. Guo, J. Yu, F. Liu, J. Sun, X. Wang, T. Wang, C. Zhao, Ni-CaO dual function materials prepared by different synthetic modes for integrated CO_2 capture and conversion, Chem. Eng. J. 428 (2022), 132110, https://doi.org/10.1016/j.cej.2021.132110.
[31] R.R. Kondakindi, G. McCumber, S. Aleksic, W. Whittenberger, M.A. Abraham, Na2CO3-based sorbents coated on metal foil: CO_2 capture performance, Int. J. Greenh. Gas. Control 15 (2013) 65–69, https://doi.org/10.1016/j.ijggc.2013.01.038.
[32] J.V. Veselovskaya, V.S. Derevschikov, O.A. T.Yu. Kardash, T.A. Stonkus, A. G. Trubitsina, Okunev, Direct CO_2 capture from ambient air using K2CO3/Al2O3 composite sorbent, Int. J. Greenh. Gas. Control 17 (2013) 332–340, https://doi.org/10.1016/j.ijggc.2013.05.006.
[33] Y. Wu, X. Chen, M. Radosz, M. Fan, W. Dong, Z. Zhang, Z. Yang, Inexpensive calcium-modified potassium carbonate sorbent for CO_2 capture from flue gas: improved SO2 resistance, enhanced capacity and stability, Fuel 125 (2014) 50–56, https://doi.org/10.1016/j.fuel.2014.02.014.